

AUTOMATED DESIGN OF PROPELLANT-OPTIMAL, END-TO-END, LOW-THRUST TRAJECTORIES FOR TROJAN ASTEROID TOURS

Jeffrey Stuart*, Kathleen Howell[†] and Roby Wilson[‡]

The Sun-Jupiter Trojan asteroids are celestial bodies of great scientific interest as well as potential resources offering water and other mineral resources for long-term human exploration of the solar system. Previous investigations under this project have addressed the automated design of tours within the asteroid swarm. This investigation expands the current automation scheme by incorporating options for a complete trajectory design approach to the Trojan asteroids. Computational aspects of the design procedure are automated such that end-to-end trajectories are generated with a minimum of human interaction after key elements and constraints associated with a proposed mission concept are specified.

INTRODUCTION

Near Earth Objects (NEOs) are currently under consideration for manned sample return missions,¹ while a recent NASA feasibility assessment concludes that a mission to the Trojan asteroids can be accomplished at a medium class, New Frontiers level.² Tour missions within asteroid swarms allow for a broad sampling of interesting target bodies either for scientific investigation or as potential resources to support deep-space human missions. However, the multitude of asteroids within the swarms necessitates the use of automated design algorithms if a large number of potential mission options are to be surveyed. Previously, a process to automatically and rapidly generate sample tours within the Sun-Jupiter L_4 Trojan asteroid swarm with a minimum of human interaction has been developed.³ This investigation extends the automated algorithm to include a variety of electrical power sources for the low-thrust propulsion system. The proposed tour creation strategy is not specific to the problem of asteroid missions and, therefore, the low-thrust tour design concept is readily applied to a diverse range of prospective mission scenarios.

High-efficiency, low-thrust propulsion systems are particularly attractive for missions to the Sun-Jupiter equilateral equilibrium points because of the relatively stable natural gravitational dynamics in these regions. Propellant-optimal, low-thrust trajectories, realized by constant specific impulse systems in nonlinear dynamical regimes, typically require coasting arcs and the careful balancing of engine capability with transfer time. The inclusion of additional coasting arcs requires engine shut-downs and restarts that may be operationally inefficient and generally infeasible. Therefore,

*Graduate Student, Purdue University, School of Aeronautics and Astronautics, 701 W. Stadium Ave., West Lafayette, IN, 47906, (765) 620-4342, jrstuart@purdue.edu.

[†]Hsu Lo Professor of Aeronautical and Astronautical Engineering, Purdue University, School of Aeronautics and Astronautics, 701 W. Stadium Ave., West Lafayette, IN, 47906, (765) 494-5786, howell@purdue.edu.

[‡]Supervisor, Inner Planet Missions Analysis Group, Mission Design and Navigation Section, Jet Propulsion Laboratory, California Institute of Technology, 4800 Oak Grove Dr., Pasadena, CA 91109, (818) 393-5301, roby.s.wilson@jpl.nasa.gov.

a variable specific impulse (VSI) engine that varies the optimal thrust magnitude is selected to simplify the generation of rendezvous solutions.⁴ As a consequence, no coasting arcs are required for rendezvous and the initial generation of optimal trajectories is less restrictive in terms of thrust duration. Examples of VSI engines include the Variable Specific Impulse Magnetoplasma Rocket (VASIMR) currently under development by the Ad Astra Rocket Company⁵ and the Electron and Ion Cyclotron Resonance (EICR) Plasma Propulsion Systems at Kyushu University in Japan.⁶

In general, the computation of locally fuel-optimal trajectories is posed as an optimal control problem. The possible formulations to solve the problem include a low-dimension but less flexible indirect approach using optimal control theory^{7,8,9} or a higher-dimension but more robust direct scheme.^{10,11,12} A combination of an indirect and a direct method is termed a hybrid optimization algorithm and exploits the relative benefits of both local optimization strategies. For this investigation, the Euler-Lagrange Theorem¹³ offers conditions for optimal engine operation while the optimization packages SNOPT¹⁴ and *fmincon* minimize propellant costs. Relatively short times-of-flight (compared to long-duration spiral trajectories), as well as continuation methods, further increase the solution stability.

Previous investigations have resulted in a scheme that generates tour sequences within the asteroid swarm, as well as an outbound, or interplanetary, leg that departs the Earth and terminates with a rendezvous at the first asteroid in the sequence.³ For the interplanetary transfer arc to the swarm, more than a low-thrust propulsion system is required for this transfer to occur in a reasonable length of time. Therefore, a V_∞ at Earth departure, delivered by conventional high-thrust chemical engines, any number of planetary fly-bys, or some combination of such external options to gain energy are incorporated. After Earth departure, the only thrust along the outbound arc in this application is delivered by the low-thrust system. This combination of low-thrust and departure V_∞ is a specific example of hybrid propulsion, i.e., the blending of various propulsion methods. By specifying that the spacecraft “arrival” condition matches the initial state along the tour path within the swarm, the two independent segments are joined into an end-to-end baseline design offering cost and timing estimates for a Trojan asteroid tour.

In this investigation, the effect of the electrical power source is examined within the context of the trajectory design and optimization procedures as well as the resulting propellant consumption and engine operation histories. Three types of electrical power source are compared:

1. constant power Nuclear Electric Propulsion, or NEP, systems,
2. varying power Solar Electric Propulsion, or SEP, thrusters,
3. and hybrid constant/varying power Power-Limited SEP, or PLS, engines.

Constant power systems typically employ an on-board source, such as radioisotope thermoelectric generators (RTGs), to deliver a consistent, but limited, supply of electrical power. In contrast, SEP systems use photons emitted by the Sun, and collected by solar cells affixed to the spacecraft, to provide electrical power. However, a potential concern for SEP spacecraft involves the Sun as a power source, i.e., photon density is inversely proportional to the square of the distance from the Sun and that extended periods of shadow must be avoided along the baseline trajectory and incorporated in any guidance algorithm. A further concern for any low-thrust propulsion system is the usual upper bound on engine power for safe operation or a peak engine efficiency power level. In either case, a limit exist upon the maximum power available to the engine, even though the solar panels on

a SEP spacecraft may collect more than sufficient electricity to exceed this bound. Thus, a power-limited SEP thruster is also investigated, where this engine type is modeled as a hybrid system of constant- and varying-power engines. The three distinct low-thrust propulsion scenarios offer a variety of challenges and opportunities, especially when implemented into the overall automated trajectory generation procedure.

SYSTEM MODELS

Two key steps are initially necessary to successfully formulate the rendezvous problem, namely the definition of the physical environment to model the dynamics of the system and the construction of the initial and target state vectors. The model for the unpowered spacecraft dynamics is independent of the low-thrust and optimization strategies and is, therefore, adjusted to introduce various levels of model fidelity.

Circular Restricted Three-Body Problem

The dynamics are initially modeled in terms of the Circular Restricted Three Body Problem (CR3BP) with the Sun as one primary and Jupiter as the second. Note that even though the spacecraft departs from the Earth and a V_∞ relative to the Earth is evaluated, Earth gravity is not accounted for in this model. The equations of motion are formulated within the context of a rotating reference frame where \hat{x} is directed from the Sun to Jupiter, \hat{z} is normal to the orbital plane of the primaries and parallel to orbital angular momentum, and \hat{y} completes the right-handed set. The origin of the coordinate system is the Sun-Jupiter barycenter. Incorporated into the forces that influence the motion in this system are terms that arise from the thrusting of the Variable Specific Impulse (VSI) engine. The system of equations are nondimensionalized to aid numerical integration efficiency: computed results are converted to dimensional quantities by the proper use of the characteristic quantities and spacecraft parameter values. The characteristic quantities are defined as the Sun-Jupiter distance, the mass of the primaries, the characteristic time, and the initial spacecraft mass. The spacecraft state vector is then defined as:

$$\chi = \begin{Bmatrix} \mathbf{r} \\ \mathbf{v} \\ m \end{Bmatrix} \quad (1)$$

where \mathbf{r} is the position vector relative to the barycenter, \mathbf{v} is the velocity vector with respect to the barycenter as viewed by a rotating observer, and m is the instantaneous mass of the spacecraft. The equations of motion are then derived with the result:

$$\dot{\chi} = \begin{Bmatrix} \dot{\mathbf{r}} \\ \dot{\mathbf{v}} \\ \dot{m} \end{Bmatrix} = \begin{Bmatrix} \mathbf{v} \\ \mathbf{f}_n(\mathbf{r}, \mathbf{v}) + \frac{T}{m} \mathbf{u} \\ -\frac{T^2}{2P} \end{Bmatrix} \quad (2)$$

where T is thrust magnitude, P is engine power, \mathbf{u} is a unit vector defining the thrust direction, and \mathbf{f}_n represents the natural acceleration of the spacecraft. Furthermore, denote the six-dimensional vector that includes position \mathbf{r} and velocity \mathbf{v} by the vector \mathbf{x} , where $\mathbf{x} = [x \ y \ z \ \dot{x} \ \dot{y} \ \dot{z}]^T$. The scalar elements of \mathbf{f}_n are then expressed in terms of the rotating frame as:

$$\mathbf{f}_n = \begin{Bmatrix} 2\dot{y} + x - \frac{(1-\mu)(x+\mu)}{d_1^3} - \frac{\mu(x+\mu-1)}{d_2^3} \\ -2\dot{x} + y - \frac{(1-\mu)y}{d_1^3} - \frac{\mu y}{d_2^3} \\ -\frac{(1-\mu)z}{d_1^3} - \frac{\mu z}{d_2^3} \end{Bmatrix} \quad (3)$$

where d_1 and d_2 are the distances to the vehicle from the Sun and Jupiter, respectively, that is

$$d_1 = \sqrt{(x + \mu)^2 + y^2 + z^2} \quad (4)$$

$$d_2 = \sqrt{(x + \mu - 1)^2 + y^2 + z^2}. \quad (5)$$

The mass parameter μ is

$$\mu = \frac{M_J}{M_S + M_J} \quad (6)$$

where M_S and M_J are the masses of the Sun and Jupiter, respectively. The power P is defined as a scalar value between zero and a maximum available power level specified by the engine model and operating conditions, such that

$$0 \leq P \leq P_{\max}. \quad (7)$$

For this investigation, the value of P_{\max} is specified in terms of a reference power level P_{ref} for NEP and SEP systems while an engine power limit P_{lim} is employed to further define a PLS system. Then, the engine thrust T is evaluated via

$$T = \frac{2P}{I_{sp}g_0} \quad (8)$$

where I_{sp} is the engine specific impulse and $g_0 = 9.80665 \text{ m/s}^2$, the gravitational acceleration at the surface of the Earth. Further information on the system and spacecraft parameters is available in Table 1.

Table 1. System and spacecraft parameter values.

Quantity	Value
Solar mass (M_S), kg	1.9891×10^{30}
Jupiter mass (M_J), kg	1.8986×10^{27}
Gravitational Constant (G), $\frac{\text{km}^3}{\text{kg} \cdot \text{sec}^2}$	6.67428×10^{-20}
Mass parameter (μ)	9.53816×10^{-4}
Sun-Jupiter distance (l^*), km	7.78412×10^8
Characteristic Time (t^*), sec	5.95911×10^7
Characteristic Time (t_d^*), days	6.89712×10^2
Reference spacecraft mass (m_r), kg	500
Reference engine power (P_{ref}), kW	1.0
Engine power limit (P_{lim}), kW	4.0

Point-Mass Ephemeris Model and Relative Equations of Motion

While the CR3BP serves as a powerful tool for initial analysis, higher fidelity models are required for more detailed and accurate investigation. A more accurate model for point masses moving under

the influence of gravity is provided by the relative vector equation of motion for a particle i moving with respect to a central body q :

$$\ddot{\mathbf{r}}_{qi} + \frac{G(m_i + m_q)}{r_{qi}^3} \mathbf{r}_{qi} = G \sum_{\substack{j=1 \\ j \neq i, q}}^n m_j \left(\frac{\mathbf{r}_{ij}}{r_{ij}^3} - \frac{\mathbf{r}_{qj}}{r_{qj}^3} \right) \quad (9)$$

where additional bodies are denoted by the subscript j . The positions and velocities of celestial bodies are available from the Jet Propulsion Laboratory's HORIZONS system.¹⁵ The relative position vector \mathbf{r}_{ij} is defined

$$\mathbf{r}_{ij} = \mathbf{r}_{qj} - \mathbf{r}_{qi} \quad (10)$$

where all positions are known relative to the central body q . Therefore, the natural dynamics of the spacecraft in an inertial frame are mathematically modeled as

$$\mathbf{f}_n(t, \mathbf{r}_{qi}) = -\frac{G(m_i + m_q)}{r_{qi}^3} \mathbf{r}_{qi} + G \sum_{\substack{j=1 \\ j \neq i, q}}^n m_j \left(\frac{\mathbf{r}_{ij}}{r_{ij}^3} - \frac{\mathbf{r}_{qj}}{r_{qj}^3} \right) \quad (11)$$

where the system is no longer time invariant. Since motion within the asteroid swarm is relatively distant from most perturbing bodies, only the Sun and Jupiter are incorporated in the ephemeris model for this preliminary investigation. Additional bodies can be readily included and the number does not alter the low-thrust engine model and the implementation of the optimization algorithm.

Initial and Target States

The computation of rendezvous arcs requires the definition of an initial state from which the spacecraft departs whenever a thrust segment is initiated and a target state that serves as a matching condition for the spacecraft state vector upon arrival. This definition is accomplished by specifying the initial state \mathbf{x}_I to be the position and velocity of a specified asteroid (or Earth, for the Earth to asteroid arc) that is considered the departure body for a particular rendezvous segment. Likewise, the target state \mathbf{x}_T is the position and velocity of the desired arrival body. In the ephemeris point-mass model in Section , the states of celestial bodies at a given epoch are determined by interpolation of the HORIZONS data. For the simplified model used in the automated tour design scheme, however, an equivalent continuous path for the celestial body is determined, where the motion satisfies the natural dynamics from the Sun-Jupiter CR3BP. Accordingly, a set of reference nodes are extracted from the HORIZONS data, transformed to the Sun-Jupiter rotating frame, and supplied as the initial guess for a multiple shooting corrections process where continuity is specified for all interior points.¹⁶ In this corrections scheme, the nodes are allowed to vary without constraint, so long as the resulting solution provides a continuous path for the asteroid motion. Figure 1 displays one such conversion, with the original HORIZONS data represented by a dashed line and the reconverged continuous CR3BP trajectory the solid line. Motion for all 10 asteroids, as well as the Earth, is transitioned to the CR3BP. Once a tour trajectory is determined within the context of the CR3BP, the results are transitioned to the point-mass ephemeris model to restore the true positions of the asteroids and the Earth.

TRAJECTORY OPTIMIZATION

A local hybrid optimization scheme is proposed wherein indirect procedures are combined with direct methods to retain low-dimensionality and, therefore, computational efficiency, while increasing the robustness of the process convergence characteristics. The application of techniques from

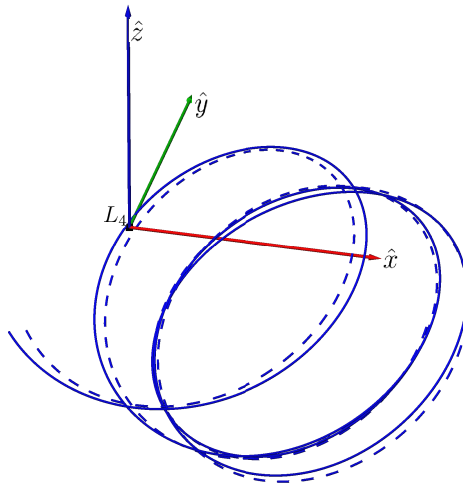


Figure 1. Path of asteroid 1143 Odysseus from Oct. 3, 2021 to Oct. 3, 2061 in Sun-Jupiter rotating frame from ephemeris data (dashed) and under CR3BP dynamics (solid)

the calculus of variations supplies conditions on optimal operation of the engine while requiring only the solution of a set of co-states. In addition to reducing the number of function evaluations per iteration, this indirect approach also ensures smooth and continuous control history while not restricting engine operation time histories to an assumed form. A spacecraft mass objective function is locally optimized using a gradient based procedure, removing a requirement to derive and employ the sensitive transversality conditions of indirect methods. Global and heuristic algorithms, though not addressed in this study, can also be used to optimize fuel performance.

Three distinct low-thrust engine types are considered in this investigation: constant power systems (e.g., NEP), varying power thrusters (e.g., SEP), and hybrid constant- and varying-power engines (e.g., PLS). While the underlying natural dynamics are unaltered, the variation in power source affects the conditions for optimal engine operation. Accordingly, for the constant-power and varying-power scenarios, the rendezvous problem is first posed indirectly using the calculus of variations for a formulation as a two-point boundary value problem (2PBVP). The engine operational states are then determined from the Euler-Lagrange equations. The two distinct sets of operating conditions and differential equations arising from the constant- and varying-power thrusters are then combined, with appropriate switching conditions, for trajectories generated using a PLS engine. For all cases, the thrust duration TD must be pre-specified when a VSI engine is employed. If no limit is placed on either the thrust duration or mass consumption, the optimization process drives TD and I_{sp} to infinity for zero propellant mass.

Indirect Optimization of Constant Power Thrust Arcs

When the on-board propulsion system is powered by a self-contained power source as is the case with a NEP engine, the maximum engine power P_{\max} is assumed to be a constant value over the duration of the mission. For all NEP trajectories considered in this investigation, the maximum engine power is specified to be $P_{\max} = P_{\text{ref}} = 1$ kW. To fully define the optimization problem, the performance index and the boundary conditions must also be specified. To arrive at the target asteroid with the maximum final spacecraft mass for a specified thrust duration, the performance

index J is defined

$$\max J = m_f. \quad (12)$$

The boundary conditions and the Hamiltonian are adjoined to the performance index, so that Eq. (12) is expanded to become the Bolza function

$$\max J' = m_f + \boldsymbol{\nu}_0^T \boldsymbol{\psi}_0 + \boldsymbol{\nu}_f^T \boldsymbol{\psi}_f + \int_{t_0}^{t_f} [H - \boldsymbol{\lambda}^T \dot{\boldsymbol{\chi}}] dt \quad (13)$$

where H is the problem Hamiltonian, $\boldsymbol{\lambda}$ is a co-state vector, the terms $\boldsymbol{\psi}$ are vectors comprised of boundary conditions, and the vector terms involving $\boldsymbol{\nu}$ are Lagrange multipliers corresponding to the boundary conditions. The co-state vector is then

$$\boldsymbol{\lambda} = \begin{Bmatrix} \boldsymbol{\lambda}_r \\ \boldsymbol{\lambda}_v \\ \lambda_m \end{Bmatrix} \quad (14)$$

where $\boldsymbol{\lambda}_r$ and $\boldsymbol{\lambda}_v$ are three-dimensional vectors comprised of the position and velocity co-states, respectively, and the scalar λ_m is the mass co-state. The initial and final vector boundary conditions are

$$\boldsymbol{\psi}_0 = \mathbf{x}_I - \mathbf{x}_I(\tau_0) = \mathbf{0} \quad (15)$$

and

$$\boldsymbol{\psi}_f = \mathbf{x}_T - \mathbf{x}_T(\tau_0 + TD) = \mathbf{0} \quad (16)$$

where the subscripts I and T indicate the states associated with the current asteroid and target asteroid, respectively. Equation (15) is implicitly satisfied by defining \mathbf{x}_I as the state along the current asteroid trajectory as defined by the parameter τ_0 . The final, or target, boundary conditions in Eq. (16) are satisfied by solving the boundary value problem.

The calculus of variations is employed to define several properties of the 2PBVP and acquire the derivatives of the co-states. The problem Hamiltonian is

$$H = \boldsymbol{\lambda}^T \dot{\boldsymbol{\chi}} = \boldsymbol{\lambda}_r^T \mathbf{v} + \boldsymbol{\lambda}_v^T \left[\mathbf{f}_n(t, \mathbf{r}, \mathbf{v}) + \frac{T}{m} \mathbf{u} \right] - \lambda_m \frac{T^2}{2P} \quad (17)$$

where the value of H is constant over the trajectory for the time invariant CR3BP. For the time varying ephemeris model, H is no longer a constant value. The optimal controls emerge by maximizing the Hamiltonian with respect to the controls T , P , and \mathbf{u} such that

$$P = P_{\max} \quad (18)$$

$$T = \frac{\lambda_v P_{\max}}{\lambda_m m} \quad (19)$$

$$\mathbf{u} = \frac{\boldsymbol{\lambda}_v}{\lambda_v} \quad (20)$$

where $\lambda_v = \|\boldsymbol{\lambda}_v\|$. Given these control expressions, the Hamiltonian is reformulated and Eq. (17) is rewritten as

$$H = \boldsymbol{\lambda}_r^T \mathbf{v} + \boldsymbol{\lambda}_v^T \mathbf{f}_n + S \cdot T \quad (21)$$

where S is the switching function

$$S = \frac{\lambda_v}{m} - \frac{\lambda_m T}{2P_{\max}}. \quad (22)$$

The Euler-Lagrange conditions for optimality modify the performance index in Eq. (13). With the reformulated Hamiltonian, that is, Eq. (21), the following equations of motion for the co-states emerge

$$\dot{\lambda} = -\left(\frac{\partial H}{\partial \chi}\right)^T = \begin{pmatrix} -\lambda_v^T \left(\frac{\partial f_n}{\partial r}\right) \\ -\lambda_r^T - \lambda_v^T \left(\frac{\partial f_n}{\partial v}\right) \\ \lambda_v \frac{T}{m^2} \end{pmatrix} \quad (23)$$

where the initial state for λ_m is set to unity to reduce the number of variables to be determined. Note that: (a) a similar procedure to minimize the initial mass for a given target mass provides identical conditions for engine operation, and (b) the differential equations for the co-states do not change form based upon the underlying natural dynamics; thus, $\frac{\partial f_n}{\partial r}$ and $\frac{\partial f_n}{\partial v}$ can be freely substituted when using models of varying fidelity.

Indirect Optimization of Varying Power Thrust Arcs

The development of the operation conditions for a varying engine power, e.g., SEP, system proceeds along the same lines as the indirect method for NEP thrusters. In contrast, however, the maximum available engine power is now determined via

$$P_{\max} = \frac{P_{\text{ref}}}{d_s^2} \quad (24)$$

where d_s is the non-dimensional distance between the spacecraft and the sun. Note that $d_s = d_1$ in the CR3BP and $d_s = \|\mathbf{r}_{qi}\|$ for ephemeris models of motion. Under this power law, the spacecraft has a nominal operating power of 1 kW while in the vicinity of the L_4 libration point but the available engine power rapidly rises as the spacecraft approaches the inner solar system. For a pure SEP system, no upper or lower limit is placed on the available engine power.

The objective function and constraints for a SEP system are the same as for NEP engines, so Eqs. (12)-(16) are unchanged in the definition of the 2PBVP. Recalling from Eq. (18) that the most efficient engine operation is at maximum available power, the new problem Hamiltonian is then

$$H = \lambda^T \dot{\chi} = \lambda_r^T \mathbf{v} + \lambda_v^T \left[\mathbf{f}_n(t, \mathbf{r}, \mathbf{v}) + \frac{T}{m} \mathbf{u} \right] - \lambda_m \frac{T^2 d_s^2}{2P_{\text{ref}}}. \quad (25)$$

As before, maximizing the Hamiltonian provides the primer vector in Eq. (20) and the thrust magnitude control

$$T = \frac{\lambda_v P_{\text{ref}}}{\lambda_m m d_s^2} \quad (26)$$

while the Euler-Lagrange conditions yield the co-state equations of motion

$$\dot{\lambda} = -\left(\frac{\partial H}{\partial \chi}\right)^T = \begin{pmatrix} -\lambda_v^T \left(\frac{\partial f_n}{\partial r}\right) + \lambda_m \frac{T^2}{P_{\text{ref}}} \mathbf{d}_s \\ -\lambda_r^T - \lambda_v^T \left(\frac{\partial f_n}{\partial v}\right) \\ \lambda_v \frac{T}{m^2} \end{pmatrix} \quad (27)$$

where \mathbf{d}_s is the distance vector from the Sun to the spacecraft ($\mathbf{d}_s = \mathbf{d}_1$ and $\mathbf{d}_s = \mathbf{r}_{qi}$ for the CR3BP and ephemeris models, respectively). As with a constant-power thrust arc, the engine operating conditions and differential equations are unchanged for the case of minimizing initial mass and for differing models of the natural dynamics.

Hybrid Optimization and Hybrid Propulsion

The design process for the overall mission trajectory is divided into two parts. The creation of the tour within the asteroid swarm is first accomplished; computation of individual rendezvous arcs is an integral component. The second step is then the generation of the interplanetary arc from Earth to the asteroid swarm. This split is used advantageously to isolate and address challenges for each of the two components without affecting the design and computation of the opposite element. However, the end conditions of the outbound segment must be carefully blended with the initial conditions of any specific rendezvous sequence. Therefore, it is natural to pose the propellant minimization problem differently for the two components, the outbound segment and the tour phase. So, for reference rendezvous arcs within the swarm, the initial spacecraft mass is specified as the reference mass from Table 1, i.e., $m_0 = m_r$. The optimization package SNOPT is then used to maximize the final mass m_f , with the additional non-linear constraints specified by Eqs. (15) and (16). Note that the same initial condition $m_0 = m_r$ is used for all baseline asteroid-to-asteroid arcs generated in the CR3BP.

As previously stated, the Earth departure leg greatly benefits from the inclusion of a hybrid propulsion scheme assuming an initial departure velocity is allowed. Propellant mass is optimized by targeting a final spacecraft mass of $m_f = m_r$ while using SNOPT to minimize the spacecraft mass at Earth departure m_0 . However, the inclusion of a departure velocity invalidates the initial boundary condition as posed in Eq. (15). Position continuity must be maintained, but velocity is now constrained, i.e.,

$$\sqrt{\Delta \mathbf{v}_I \cdot \Delta \mathbf{v}_I} - V_\infty = 0 \quad (28)$$

where $\Delta \mathbf{v}_I = \mathbf{v}_I - \mathbf{v}_\oplus(\tau_0)$, such that \mathbf{v}_I is the spacecraft initial velocity and $\mathbf{v}_\oplus(\tau_0)$ is defined as the velocity of Earth at spacecraft departure. The departure V_∞ is selected based upon the capabilities of a chemical booster stage or hyperbolic velocity after an Earth fly-by. Thus, for the interplanetary leg, SNOPT minimizes the initial spacecraft mass m_0 subject to the constraints given in Eqs. (16) and (28) and position continuity with the Earth at the initial departure epoch.

AUTOMATED TOUR CREATION

A mission to the vicinity of the Sun-Jupiter ‘‘Greek’’ or ‘‘Trojan’’ asteroid families will almost certainly entail rendezvous with and the observation of multiple objects. Recall that the asteroid tour is determined prior to the generation of an Earth-to-asteroid outbound segment. A previous investigation in this project proposed a strategy to rapidly and automatically generate a large number of candidate asteroid tours satisfying a set of constraints.³ This trajectory evaluation scheme uses CR3BP dynamics and a NEP system and therefore yields only approximate propellant costs. The asteroid swarm rendezvous sequences in the current investigation are constructed using the preliminary design scheme and then further refined by adjusting the dynamical fidelity and propulsion system parameters to realize more accurate timing and propellant requirements.

Outbound Leg Generation

For a specific Trojan tour of interest, an Earth-to-swarm segment must be included such that the spacecraft rendezvous with the first asteroid in the tour occurs prior to the defined asteroid arrival epoch. As previously stated, this arc is enabled by the use of a hybrid propulsion scheme where an initial Earth-departure V_∞ is specified. Recall that the objective of the optimization procedure for this leg is the minimization of the initial spacecraft mass subject to the constraint that the mass

upon asteroid arrival equals 500 kg. This phase of the trajectory design process is also automated by creating a library of pre-generated trajectory arcs using CR3BP dynamics and a NEP engine. So, point solutions for locally optimal rendezvous arcs between Earth and each of the 10 sample asteroids are computed where the departure epoch τ_d occurs within the year 2018 and the spacecraft arrives in the vicinity of the asteroid swarm 3.5 years later in 2021. Thereafter, for any specific tour, the pre-computed departure epoch is adjusted by a integer multiple of the Earth-Jupiter synodic period, that is, 398.88 days, such that the spacecraft arrives at the initial asteroid only a short time in advance of the selected starting epoch for the asteroid tour.

The outbound leg effected using a power-limited SEP system provides a challenge in that the engine will have to switch engine models from a constant-power regime defined by the fixed maximum engine power to a varying-power domain where the sun distance determines the available power. In this investigation, the switch between thrust regimes is accomplished by introducing an intermediate patch point along the thrust arc, where the node is defined by the state χ_s and co-state λ_s . Prior to the switch point, the spacecraft engine operates with constant power $P_{\max} = P_{\lim}$ while after the switch point the varying power is given by $P_{\max} = \frac{P_{\text{ref}}}{d_s^2}$, where the appropriate control laws and co-state equations of motion are used. However, care must be taken to ensure that this switch occurs when the power available from the sun matches the limit on maximum engine power. Accordingly, the constraint

$$\frac{P_{\text{ref}}}{d_s^2} - P_{\lim} = 0 \quad (29)$$

is included when generating trajectories using a PLS system. Additional constraints on the PLS enabled trajectory include:

$$t_c + t_v - TD_{out} = 0 \quad (30)$$

and, for trajectories using ephemeris dynamical models

$$\tau_s - \tau_d - t_c = 0 \quad (31)$$

where t_c is the time spent thrusting under constant power, t_v the duration under varying power, TD_{out} the total thrust interval on the outbound leg, τ_s the switch epoch, and τ_d the epoch at Earth departure. Continuity in state is ensured by

$$\chi_s^t - \chi_s = 0 \quad (32)$$

where χ_s^t corresponds to the spacecraft state at the end of the constant-power thrust arc and χ_s is the initial state of the varying-power segment. During preliminary optimization runs, no restriction was placed on continuity in the co-state λ_s , however, the naturally emerging optimal solution resulted in co-state continuity across the two thrust domains. Accordingly, the constraint

$$\lambda_s^t - \lambda_s = 0 \quad (33)$$

is also included for PLS outbound legs, where the addition of this constraint has the positive side effect of improving convergence of the numerical optimization. This result also indicates the more straight-forward implementation of removing the switching node and instead constructing a set of equations of motion wherein the switch in engine power domain is handled as an automatic function of the spacecraft position.

Scaling Results

A convenient method of generating initial guesses for optimization is to scale the results of pre-existing solutions. In this investigation the initial conditions of the rendezvous arcs computed using the CR3BP and NEP thruster are scaled in order to improve convergence upon a locally optimal solution. The following set of *approximate* relations are used when the engine operating power is altered

$$m_{c2} \approx \frac{P_1}{P_2} m_{c1} \quad (34)$$

$$\lambda_2 \approx \frac{P_1}{P_2} \lambda_1 \quad (35)$$

where m_c is the mass consumed along the thrust arc, $m_c = m_0 - m_f$. On the other hand the relations

$$m_{c2} \approx \left(\frac{m_{0,2}}{m_{0,1}} \right)^2 m_{c1} \quad (36)$$

$$\lambda_2 \approx \frac{m_2}{m_1} \lambda_1 \quad (37)$$

are used when altering the spacecraft mass. These two sets of scaling equations are used in conjunction when the both the spacecraft mass and the engine power are changed. In addition to the construction of initial guesses, the scaling relations are useful as a tool for rapidly examining a large variety of mission scenarios without the need to fully optimize the corresponding trajectories.

Higher-Fidelity Models

Transitioning any solution or design to an ephemeris model is a key step for validation of the results. Given a possible asteroid tour mission, the cost as well as timing estimates and engine operation histories are obtained using a corrections algorithm in the point mass ephemeris model. For the tour within the swarm, accurate propellant costs are determined by incorporating the propellant consumed along previous thrust arcs, rather than assuming each thrust arc to be independent. For example, after arrival in the swarm, the first rendezvous arc between asteroids consumes propellant mass such that the initial spacecraft mass is less than 500 kg at the initiation of the second thrust arc. Accordingly, the optimization problem for the second asteroid-to-asteroid rendezvous arc possesses an ‘initial’ spacecraft mass equal to the arrival mass at the end of the previous rendezvous segment. The propellant usage computation then continues throughout the tour in the swarm. The spacecraft mass at swarm arrival is still specified to be 500 kg and, therefore, the Earth-to-asteroid arc still targets an arrival mass of 500 kg. For this investigation, only the gravity of the Sun and Jupiter are incorporated in the point mass ephemeris model; the gravitational effect of other celestial bodies, e.g. the Earth and Mars, are assumed to be negligible, even along the outbound leg.

SAMPLE ASTEROID TOUR TRAJECTORY: 1143 ODYSSEUS

A sample asteroid tour trajectory is examined, where the spacecraft rendezvous’ with the asteroids 1143 Odysseus, 5652 Amphimachus, and 659 Nestor in sequence. A baseline set of thrust and coast arcs is constructed in the spatial CR3BP using the automated tour selection scheme,³ where the spacecraft departs the Earth in 2022 and has a mission lifetime of 10 years. The reference solution is then converged into three end-to-end trajectories in the ephemeris model, where each trajectory

is defined by the engine model used, i.e., NEP, SEP, or PLS. In all cases, however, the spacecraft is constrained to have an Earth-departure excess velocity of $V_\infty = 7.5$ km/sec and is specified to rendezvous with 1143 Odysseus 3.5 years after departing the Earth.

The three mission scenarios are analyzed in terms of propellant consumption, mission timing, and the equivalent ΔV costs of the thrust arcs. The estimated end-to-end costs as well as departure and arrival time histories are summarized in Tables 2 and 3. Note that all propulsion systems deliver approximately the same final spacecraft mass. However, each mission scenario entails a different Earth departure mass, where the NEP system requires the most propellant, the pure SEP engine the least, and the hybrid PLS thruster consumes slightly more propellant than the SEP. As can be seen in Table 3, all potential tours possess roughly equivalent timings, with departure and arrival epochs varying on the order of days or a few weeks. Note also that the SEP and PLS trajectories are nearly equivalent within the asteroid swarm itself, as is expected because both are operating as varying-power systems during this phase of the mission. The equivalent ΔV cost for each thrust segment, computed via the definition

$$\Delta V = \int_{t_0}^{t_1} \frac{T}{m} dt, \quad (38)$$

is presented in Table 4, where the initial departure V_∞ is not included in the ΔV tabulation. Because all three mission scenarios have a nominal engine operating power of 1 kW while in the L_4 region, the asteroid-to-asteroid thrust arcs generate a similar amount of ΔV regardless of engine type. In contrast the ΔV s for the outbound legs vary non-trivially between the engine types, where the trend is opposite that for the departure mass.

Table 2. Spacecraft propellant budget for 10-year mission with tour of 3 asteroids

Quantity	Value			Units
	Eph. NEP	Eph. SEP	Eph. PLS	
Mass at Earth departure	582.273	546.827	549.008	kg
Mass at final asteroid arrival	473.584	475.469	475.469	kg
Total propellant consumption	108.689	71.358	73.540	kg
V_∞ at Earth departure	7.50000	7.50000	7.50000	km/sec

In addition to propellant budgets and trajectory timeline, the physical path of the spacecraft is also of interest. Accordingly, the spacecraft trajectories under the varying propulsion systems are displayed in Fig. 2 and Fig. 3 in the inertial and Sun-Jupiter rotating frames, respectively. The Earth-to-asteroid arc is red for the NEP thruster, the SEP arc is indicated in yellow, and the PLS enabled outbound leg is orange. Arcs where the engine is operating within the swarm are dark gold, and coasts in the vicinity of asteroids are indicated by light green. The position of the Earth is displayed at the Earth departure epoch of July 17, 2022. Furthermore, in Fig. 3 Mars is shown at the point of closest spacecraft approach, where the relative proximity of the planet implies the possibility of a propellant-saving fly-by maneuver. Note that the outbound legs for the SEP and PLS mission scenarios are very similar in the physical path that they trace through space.

Time histories of the engine operating parameters such as thrust, specific impulse, and electrical power are also of great interest in mission analysis. These histories are plotted in Figs. 4, 5, and

Table 3. Epochs of interest for 10-year mission with tour of 3 asteroids

Description	Gregorian Date YYYY:MM:DD:HH:MM:SS		
	Eph. NEP	Eph. SEP	Eph. PLS
Earth departure	2022:7:17:7:34:26	2022:7:13:1:39:54	2022:7:11:5:58:16
1143 Odysseus arrival	2026:1:15:16:34:26	2026:1:11:10:39:54	2026:1:9:14:58:16
1143 Odysseus departure	2027:2:6:4:32:17	2027:2:6:12:4:49	2027:2:6:11:57:41
5652 Amphimachus arrival	2029:8:18:9:39:52	2029:8:18:17:12:24	2029:8:18:17:5:16
5652 Amphimachus departure	2030:4:29:19:18:52	2030:4:16:3:7:46	2030:4:16:3:43:23
659 Nestor arrival	2032:11:9:0:26:27	2032:10:26:8:15:21	2032:10:26:8:50:58

Table 4. Equivalent mission ΔV for 10-year mission with tour of 3 asteroids

Description	Value, km/sec		
	Eph. NEP	Eph. SEP	Eph. PLS
Earth to 1143 Odysseus	7.82336	8.60175	8.17866
1143 Odysseus to 5652 Amphimachus	1.94597	1.93721	1.93721
5652 Amphimachus to 659 Nestor	3.39160	3.40820	3.40820

6, respectively. The Earth-to-1143 Odysseus segments are indicated in magenta, the 1143 Odysseus to 5652 Amphimachus arc is green, and the 5652 Amphimachus to 659 Nestor leg is red. The discontinuities in the PLS outbound segment time histories are due to the switch in thrust regime. As is apparent in Fig. 4, each propulsion system maintains a consistent thrust order of magnitude across all thrust arcs. As expected from the excess power available, the SEP and PLS engines deliver large spikes in specific impulse over the relatively constant I_{sp} of the NEP thruster. Also of note is that the PLS and SEP systems have the same qualitative behavior, with large initial peaks in specific impulse and engine power and subsequent peaks in thrust magnitude for the outbound legs and, once the spacecraft is within the asteroid swarm, the engine operating at a nominal 1 kW of power. For all engine types, with proper adjustments for spacecraft mass and timing, these tours can serve as a reference paths for trajectory design with currently available constant specific impulse engines.

CONCLUSIONS

An automated algorithm to generate asteroid tour missions has been extended to incorporate several categories of low-thrust, variable specific impulse propulsion systems. While applied to the construction of Sun-Jupiter Trojan asteroid survey missions, the procedure is not limited by dynamical regime and is readily extended to other mission architectures. Nuclear electric and solar electric propulsion are modeled as constant- and varying-power systems, respectively, while a power-limited SEP engine is analyzed as a hybrid system of constant- and varying-power thrust regimes. Baseline trajectories computed using the CR3BP and a NEP engine are scaled appropriately by the desired engine type and available engine power and optimized in a point-mass ephemeris model of mo-

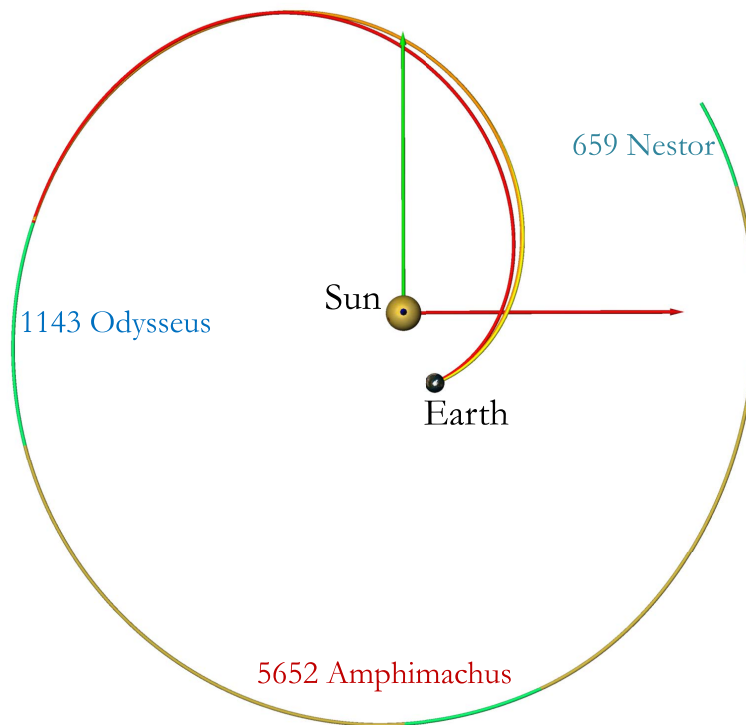


Figure 2. Plot of inertial trajectories for tours with initial target 1143 Odysseus, out-bound legs (red, orange, yellow), thrust arcs (gold), coasts in the vicinity of asteroids (green).

tion. Engine operation is determined by an indirect, calculus of variations optimization approach, where the constant- and varying-power systems follow distinct control laws and equations of motion. Results indicate that optimal operation of a PLS hybrid system implies continuity in the Euler-Lagrange co-states across a switch in thrust regime, an observation that can reduce implementation time and computational overhead. This continuity also suggests that the indirect optimization methods reveal optimal paths through space, regardless of thrust system or switches in engine operation domains. Furthermore, scaling relations for engine operation and performance quantities offer an avenue for rapid investigation of mission scenarios and spacecraft parameters.

Several avenues are open for further investigation and refinement. In particular, higher fidelity modeling of celestial body motion will increase the accuracy of the resulting designs for both the asteroid-to-asteroid arcs as well as the end-to-end tour trajectory. Of particular importance is increased fidelity in the vicinity of the Earth-Moon region and of any near passages of other massive bodies, such as Mars. The automated procedure may be further enhanced to identify close passages and fly-bys of intermediate objects in the solar system, e.g. other asteroids within the swarm or along the outbound leg from Earth. Furthermore, additional asteroids of interest may be included in the initial survey, and reliance on pre-computed libraries of solutions can be reduced or eliminated altogether. Finally, the automated procedure may be applied to other scenarios requiring multiple low-thrust or hybrid propulsion arcs, whether as part of a baseline or an extended trajectory design.

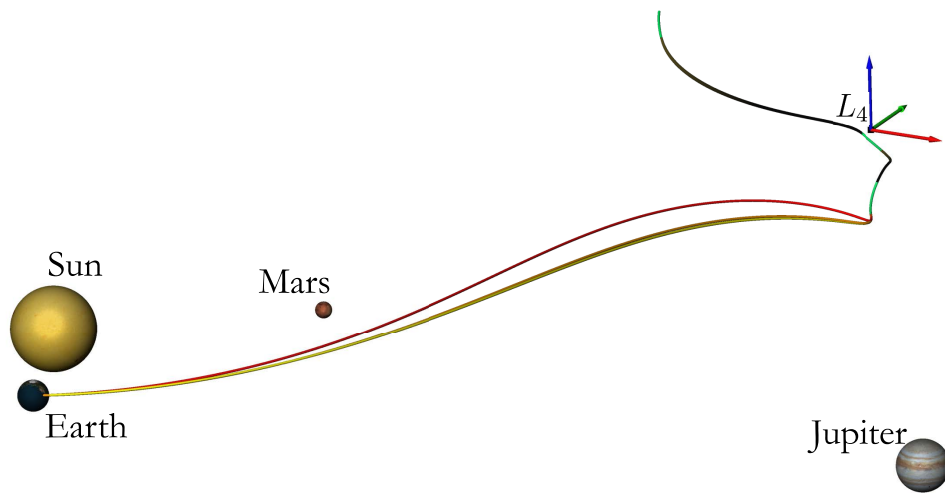


Figure 3. Plot of Sun-Jupiter rotating frame trajectories for tours with initial target 1143 Odysseus, outbound legs (red, orange, yellow), thrust arcs (black), coasts in the vicinity of asteroids (green).

ACKNOWLEDGEMENTS

This work was conducted at Purdue University and the Jet Propulsion Laboratory and is supported by the Purdue Research Foundation and a NASA Office of the Chief Technologist’s Space Technology Research Fellowship, NASA Grant NNX12AM61H. Many thanks to Wayne Schlei, who helped immensely with the trajectory images, and the people of the Jet Propulsion Laboratory, Mission Design and Navigation Section.

REFERENCES

- [1] N. Augustine, W. Austin, C. Chyba, C. Kennel, B. Bejmuk, E. Crawley, L. Lyles, L. Chiao, J. Greason, and S. Ride, “Seeking a Human Spaceflight Program Worthy of a Great Nation,” tech. rep., U.S. Human Spaceflight Plans Committee, 2009.
- [2] M. Brown, “Mission Concept Study: Trojan Tour Decadal Study,” tech. rep., National Aeronautics and Space Administration, 2011.
- [3] J. Stuart and K. Howell, “An Automated Search Procedure to Generate Optimal Low-Thrust Rendezvous Tours of the Sun-Jupiter Trojan Asteroids,” *23rd International Symposium on Spaceflight Dynamics*, Pasadena, CA, October 29 - November 4 2012.
- [4] D. Goebel, J. Brophy, J. Polk, I. Katz, and J. Anderson, “Variable Specific Impulse High Power Ion Thruster,” *Joint Propulsion Conference*, Tucson, Arizona, AIAA/ASME/SAE/ASEE, July 2005. Paper No. AIAA 2005-4246.
- [5] A. A. R. Company, “VASIMR Technology,” Accessed: November 28, 2010.
- [6] K. Komurasaki, Y. Arakawa, and H. Takegahara, “An Overview of Electric and Advanced Propulsion Activities in Japan,” *Proceedings of Third International Conference of Spacecraft Propulsion*, Cannes, France, October 2000, pp. 27–39.
- [7] M. Volle, “Optimal Variable-Specific-Impulse Rendezvous Trajectories Between Halo Orbits,” *International Symposium on Space Flight Dynamics*, Kanazawa, Japan, Japan Society for Aeronautical and Space Sciences and ISTS, June 2006. Paper No. ISTS 2006-d-73.
- [8] R. Russell, “Primer Vector Theory Applied to Global Low-Thrust Trade Studies,” *Journal of Guidance, Control, and Dynamics*, Vol. 30, March-April 2007, pp. 460–473.
- [9] J. Senent, C. Ocampo, and A. Capella, “Low-Thrust Variable-Specific-Impulse Transfers and Guidance to Unstable Periodic Orbits,” *Journal of Guidance, Control, and Dynamics*, Vol. 28, March-April 2005, pp. 280–290.

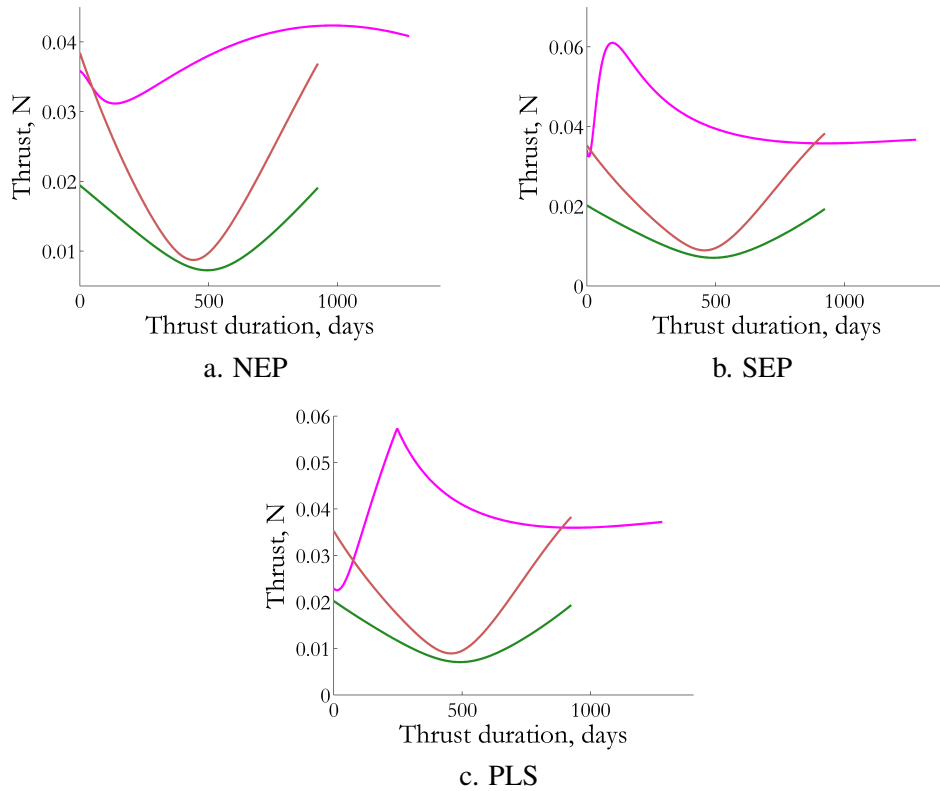


Figure 4. Thrust profiles for outbound leg (pink) and first (green) and second (red) asteroid rendezvous arcs for mission scenario with initial asteroid 1143 Odysseus.

- [10] G. Mingotti, F. Topputo, and F. Bernelli-Zazzera, “Combined Optimal Low-Thrust and Stable-Manifold Trajectories to the Earth-Moon Halo Orbits,” *New Trends in Astrodynamics and Applications III*, Vol. 886, February 2007, pp. 100–112.
- [11] C. Martin and B. Conway, “Optimal Low-Thrust/Invariant Manifold Earth Moon Transfer Trajectories,” *Space Flight Mechanics Meeting*, San Diego, California, AAS/AIAA, February 2010. Paper No. AAS 10-105.
- [12] J. Betts, “Survey of Numerical Methods for Trajectory Optimization,” *Journal of Guidance, Control, and Dynamics*, Vol. 21, March-April 1998, pp. 193–207.
- [13] A. E. Bryson, Jr. and Y.-C. Ho, *Applied Optimal Control*. Waltham, Massachusetts: Blaisdell Publishing, 1969.
- [14] P. E. Gill, W. Murray, and M. A. Saunders, “SNOPT: An SQP algorithm for large-scale constrained optimization,” *Society for Industrial and Applied Mathematics Journal of Optimization*, Vol. 12, 2002, pp. 979–1006.
- [15] Solar System Dynamics Group, *HORIZONS System*. Jet Propulsion Laboratory. <http://ssd.jpl.nasa.gov/?horizons>.
- [16] H. B. Keller, *Numerical Solution of Two Point Boundary Value Problems*. Philadelphia, Pennsylvania: Society for Industrial and Applied Mathematics, 1976.

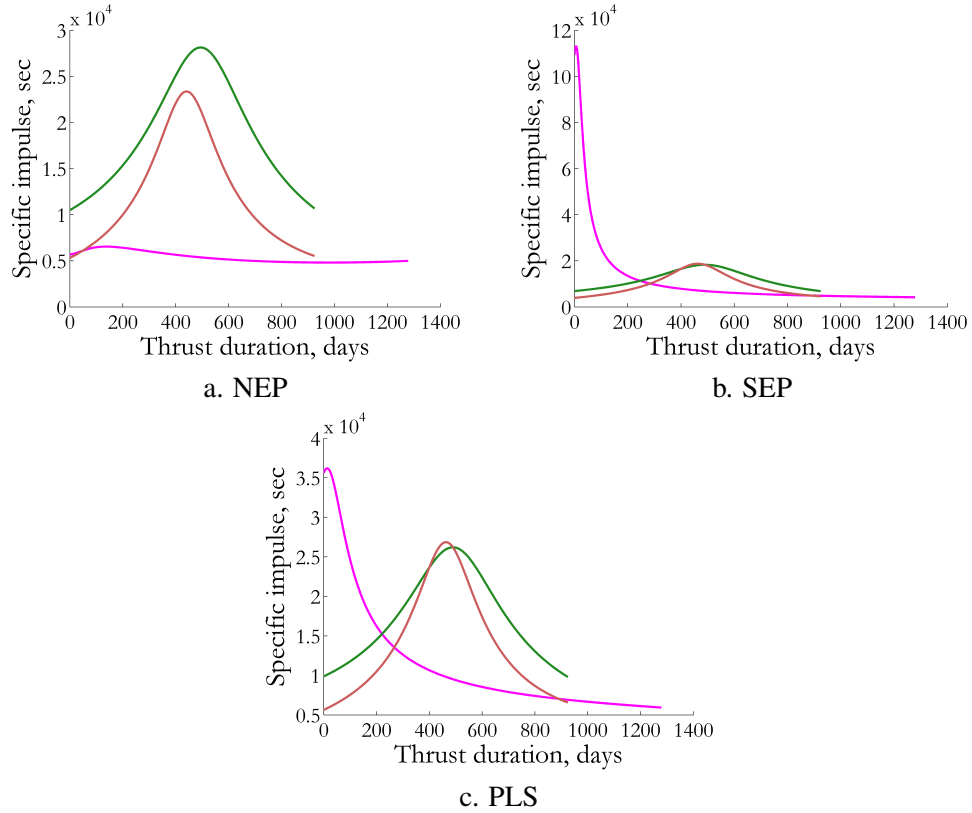


Figure 5. Specific impulse profiles for outbound leg (pink) and first (green) and second (red) asteroid rendezvous arcs for mission scenario with initial asteroid 1143 Odysseus.

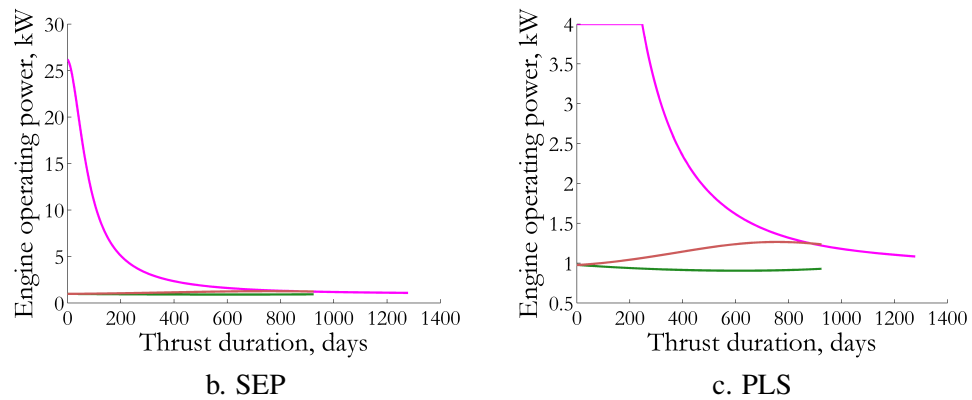


Figure 6. Operating power profiles for outbound leg (pink) and first (green) and second (red) asteroid rendezvous arcs for mission scenario with initial asteroid 1143 Odysseus. Time histories for the NEP system are constant at 1 kW and are not shown.